




Hypoxia-Inducible Factor Signaling in Macrophages Promotes Lymphangiogenesis in *Leishmania major* Infection

Anne Bowlin,^a Hayden Roys,^a Humphrey Wanjala,^a Manjunath Bettadapura,^a Gopinath Venugopal,^a Jessica Surma,^a M. Celeste Simon,^b  Tiffany Weinkopff^a

^aDepartment of Microbiology and Immunology, College of Medicine, University of Arkansas for Medical Sciences, Little Rock, Arkansas, USA

^bAbramson Family Cancer Research Institute, Department of Cell and Developmental Biology, Perelman School of Medicine, University of Pennsylvania, Philadelphia, Pennsylvania, USA

Anne Bowlin and Hayden Roys contributed equally to this work. The co-first authors are listed alphabetically.

ABSTRACT Vascular remodeling is a phenomenon seen in the cutaneous lesions formed during infection with *Leishmania* parasites. Within the lesion, *Leishmania major* infection leads to the infiltration of inflammatory cells, including macrophages, and is associated with hypoxic conditions and lymphangiogenesis in the local site. This low-oxygen environment is concomitant with the expression of hypoxic inducible factors (HIFs), which initiate the expression of vascular endothelial growth factor-A (VEGF-A) in macrophages during the infection. Here, we found that macrophage hypoxia is elevated in the skin, and the HIF target *Vegfa* is preferentially expressed at the site of infection. Further, transcripts indicative of both HIF-1 α and HIF-2 α activation were increased at the site of infection. Given that HIF mediates VEGF-A and that VEGF-A/VEGFR-2 signaling induces lymphangiogenesis, we wanted to investigate the link between myeloid HIF activation and lymphangiogenesis during *L. major* infection. We show that myeloid aryl hydrocarbon receptor nuclear translocator (ARNT)/HIF/VEGF-A signaling promotes lymphangiogenesis (the generation of newly formed vessels within the local lymphatic network), which helps resolve the lesion by draining away inflammatory cells and fluid. Concomitant with impaired lymphangiogenesis, we find the deletion of myeloid ARNT/HIF signaling leads to an exacerbated inflammatory response associated with a heightened CD4⁺ Th1 immune response following *L. major* infection. Altogether, our data suggest that VEGF-A-mediated lymphangiogenesis occurs through myeloid ARNT/HIF activation following *Leishmania major* infection and this process is critical in limiting immunopathology.

KEYWORDS ARNT, HIF, *Leishmania*, leishmaniasis, lymphangiogenesis, lymphatic vessels, macrophages, vascular remodeling

Leishmaniasis is an inflammatory disease caused by obligate intracellular protozoan parasites of the *Leishmania* species. Globally, the incidence of cutaneous leishmaniasis is 700,000 to 1.2 million new cases each year (1). More than 90 countries in Asia, Africa, and Latin America have at-risk populations, predominantly in rural areas (CDC). The parasites are transmitted by sand flies, and different species of *Leishmania* cause distinct clinical manifestations of the disease. Leishmaniasis can present in multiple forms, including visceral leishmaniasis (which is systemic and fatal if left untreated), cutaneous leishmaniasis, and mucocutaneous leishmaniasis (which results from parasite dissemination following the development of a primary cutaneous lesion). Cutaneous leishmaniasis manifests in lesions on the skin that vary from moderate papules or nodules to severe, large ulcerated lesions. The lack of a vaccine and the long duration and toxic nature of current chemotherapeutic treatments (that are often ineffective) make it very difficult to address lesion formation and the global burden of leishmaniasis (2).

Citation Bowlin A, Roys H, Wanjala H, Bettadapura M, Venugopal G, Surma J, Simon MC, Weinkopff T. 2021. Hypoxia-inducible factor signaling in macrophages promotes lymphangiogenesis in *Leishmania major* infection. *Infect Immun* 89:e00124-21. <https://doi.org/10.1128/IAI.00124-21>.

Editor Jeroen P. J. Saeij, UC Davis School of Veterinary Medicine

Copyright © 2021 American Society for Microbiology. All Rights Reserved.

Address correspondence to Tiffany Weinkopff, tweinkopff@uams.edu.

Received 4 March 2021

Returned for modification 27 April 2021

Accepted 11 May 2021

Accepted manuscript posted online 24 May 2021

Published 15 July 2021

During cutaneous and mucocutaneous leishmaniasis, the severity of disease depends on both parasite replication and the host immune response (3–8). While the CD4⁺ Th1 immune response contributes to parasite control, the overall inflammatory response can also exacerbate and prolong the pathology of the lesion (2). Over the course of infection, inflammatory monocytes and neutrophils are recruited to leishmanial lesions in massive numbers, and the recruited monocytes can differentiate into macrophages, thereby replenishing the dermal macrophage population in the tissue (9–11). To resolve the lesion, dermal macrophages respond to gamma interferon (IFN- γ) from CD4⁺ Th1 cells by producing nitric oxide (NO) that kills parasites and by expressing growth factors such as VEGF-A that expand the lymphatic vasculature to drain away cells and fluid sequestered in the lesions (12). As in other chronic inflammatory diseases, such as inflammatory bowel disease or rheumatoid arthritis, changes in the lymphatic vasculature via lymphangiogenesis can be beneficial. New lymph vessel formation in damaged tissue can help reduce inflammation by clearing excess fluid and proinflammatory cytokines (13).

Leishmania infection is generally characterized by a low-oxygen environment within the inflamed tissue (14). In inflammatory diseases such as inflammatory bowel disease or ulcerative colitis, the pathological lesions are also characterized by tissue hypoxia, which can promote the severity of disease (15, 16). Within hypoxic settings, several transcription factors, including hypoxia-inducible factors (HIF-1 α and HIF-2 α) are induced by decreased oxygen availability (17). For HIF activation, HIF- α subunits bind aryl hydrocarbon receptor nuclear translocator (ARNT; also known as HIF-1 β), and ARNT/HIF- α heterodimers translocate to the nucleus, where they induce the transcription of HIF-target genes (17). During cutaneous leishmaniasis, lesions from human patients contain elevated levels of HIF-1 α and the HIF target *Vegfa* (18–20). Activated HIF-1 α in dermal myeloid cells contributes to parasite control through the production of NO during murine *L. major* infection (19). Schatz et al. elegantly showed that both inflammatory signaling and low oxygen tension in the tissue could promote HIF-1 α accumulation in *L. major*-infected macrophages (19). However, the importance of HIF signaling beyond NO production was not investigated. Given that HIF activation can influence the expression of hundreds of genes, we explored the influence of HIF signaling on VEGF-A, which promotes lymphangiogenesis during leishmaniasis.

During *Leishmania* infection, lymphangiogenesis is required for lesion resolution (21). Macrophages produce VEGF-A that binds to VEGFR-2 on lymphatic endothelial cells (ECs) to induce their proliferation and lymphangiogenesis (12, 21). We showed previously that myeloid ARNT/HIF signaling mediates macrophage VEGF-A production during *L. major* infection, but the link between myeloid ARNT/HIF signaling and lymphangiogenesis remains undefined (12). Mice deficient in the myeloid ARNT/HIF pathway display larger lesions compared to controls, despite no differences in parasite burden (12). These results are consistent with previous findings that VEGF-A/VEGFR-2 blockade leads to larger lesions with no differences in parasite number (21). Therefore, we hypothesize that HIF-mediated production of VEGF-A by macrophages drives lymphangiogenesis and lesion resolution. Furthermore, the larger lesions in mice deficient in myeloid ARNT/HIF signaling were associated with an enhanced inflammatory infiltrate, characterized by higher numbers of inflammatory Ly6C⁺ monocytes in the lesion (12), suggesting that increased recruitment of immune cells into the inflamed tissue or impaired egress of cells out of the tissue may contribute to the immunopathology.

Given the importance of lymphangiogenesis in lesion resolution during cutaneous leishmaniasis, we investigated the role of myeloid ARNT/HIF signaling in lymphatic remodeling. We found that macrophages experience hypoxic conditions at the cellular level in the skin, and VEGF-A and other transcripts indicative of both HIF-1 α and HIF-2 α activation were elevated at the site of *L. major* infection. ARNT/HIF signaling promoted lymphatic remodeling, further supporting a role for this pathway in lesion resolution. Altogether, these results show that in addition to the well-characterized

role of macrophages in parasite killing, macrophages limit immunopathology by orchestrating lymphatic remodeling within the skin during leishmaniasis.

RESULTS

Dermal *Leishmania* lesions have been reported to exhibit hypoxia at the tissue level (14), but the hypoxic signature of individual cells has not been investigated. Therefore, we aimed to determine if hypoxic conditions could contribute to the HIF activation detected in leishmanial lesions in mice. Pimonidazole staining is regularly used to define hypoxic tissue (22). Therefore, pimonidazole staining was coupled with flow cytometry to determine if cells experienced hypoxic conditions at the cellular level following *L. major* infection. We found that dermal macrophages exhibited pimonidazole staining, regardless if the ears were infected or uninfected; CD45⁺ CD11b⁺ Ly6G⁻ CD64⁺ macrophages from inflamed infected ears and uninfamed uninfected contralateral ears displayed similar pimonidazole median fluorescence intensities (MFIs) (Fig. 1A, C, and D). Furthermore, macrophages in the skin exhibited higher levels of pimonidazole staining than macrophages in the corresponding draining lymph node (dLN) or spleen of the same mouse (Fig. 1B to D). These findings were significant at both 1 week postinfection (p.i.) (Fig. 1C) and 5 weeks p.i. (Fig. 1D). Even though dermal macrophages exhibited a higher level of pimonidazole staining than macrophages in other organs, which was expected given the skin is more hypoxic than other organs, we were surprised there was no significant difference in staining between macrophages from infected and contralateral uninfected ears. However, this experiment assumed that the macrophage population in the inflamed tissue was homogenous and that all macrophages had been in the tissue for the same amount of time. Because many macrophages are derived from Ly6C^{hi} inflammatory monocytes that infiltrate *Leishmania* lesions from the blood (9–11), we hypothesized that Ly6C^{hi} macrophages have a different hypoxic profile than Ly6C^{lo} macrophages. Given that inflammatory monocytes lose Ly6C expression as they differentiate into macrophages in lesions (9–11), we used Ly6C to distinguish macrophages that had just arrived at the lesion from macrophages already residing in the tissue. Following *L. major* infection, we found Ly6C^{lo} macrophages displayed higher levels of pimonidazole staining than Ly6C^{hi} macrophages in the same infected ear, suggesting that Ly6C^{lo} macrophages are more hypoxic than cells recently recruited from the blood (Fig. 1E and F). Altogether, these findings suggest macrophages in the skin experience hypoxic conditions at the cellular level and these hypoxic conditions may influence the activation and function of macrophages in inflamed skin during *L. major* infection.

Given that we found the skin to be more hypoxic than other organs, we investigated HIF expression in the skin and dLN during *L. major* infection. The dLN was examined in parallel to the skin as a control, given the dLN is less hypoxic, but still comes from the same mouse and is also a site with an ongoing immune response. Because *Vegfa* expression can be mediated by HIF-1 α or HIF-2 α signaling, and the relevant HIF pathway inducing lymphangiogenesis during leishmaniasis is unknown, the expression of *Hif1 α* and *Hif2 α* was examined in the skin of infected and contralateral ears and dLNs from C57BL/6 mice following inoculation with *L. major*. We found that both *Hif1 α* and *Hif2 α* were expressed at higher levels in the skin than in corresponding dLNs following infection (Fig. 2A and B). Furthermore, both HIF- α isoforms were expressed at higher levels in the skin than in the dLN, independent of the infection status of the ear. However, only *Hif1 α* expression increased in the skin after infection (Fig. 2A), while *Hif2 α* expression decreased (Fig. 2B).

Given HIF is constitutively expressed but also continuously degraded in normoxic conditions, HIF expression does not directly correlate with HIF activation. We examined the expression of *Vegfa*, a pan-HIF target and mediator of lymphangiogenesis. Consistent with previous findings, *Vegfa* was elevated in the skin with infection compared to uninfamed skin (Fig. 2C). *Vegfa* was also expressed at higher levels in the skin than in corresponding dLNs, irrespective of the infection status of the ear (Fig. 2C).

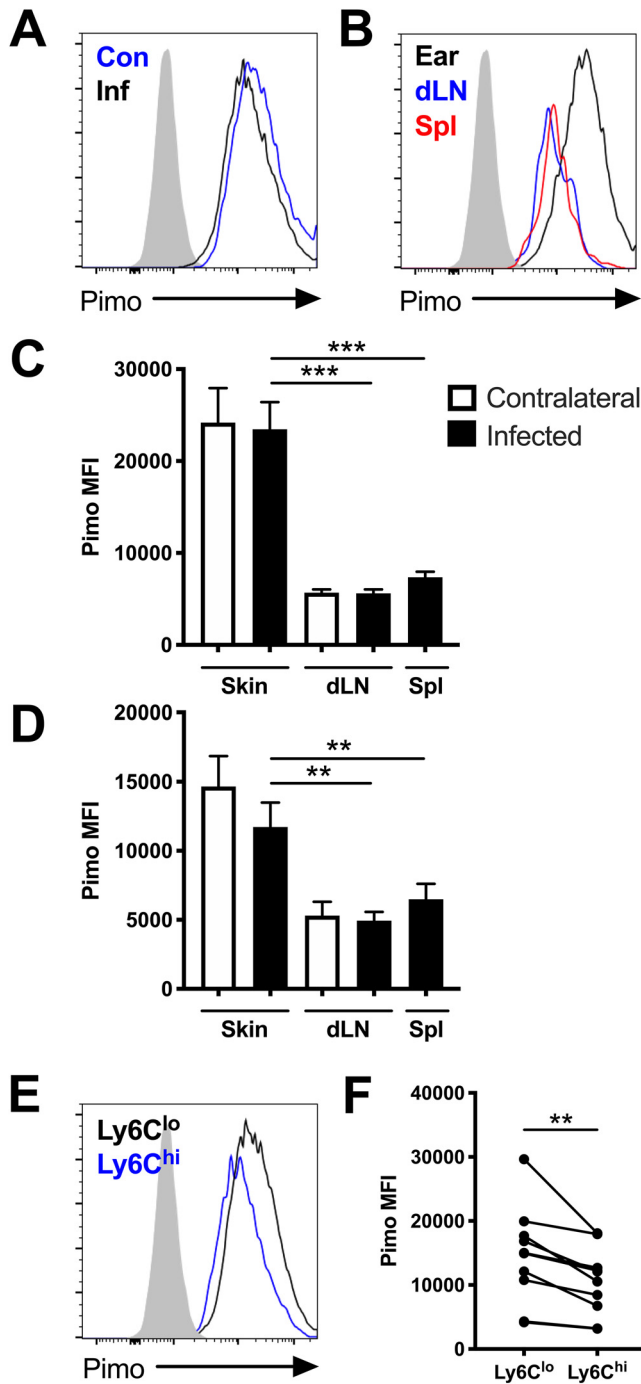


FIG 1 Macrophages experience hypoxic conditions within the site of infection following *L. major* inoculation *in vivo*. C57BL/6 mice were infected with *L. major* parasites intradermally in the ear. At 1 and 5 weeks p.i., infected and contralateral ears, infected and contralateral dLNs, and spleens were stained with pimonidazole and analyzed by flow cytometry. (A) Representative flow cytometry histograms showing pimonidazole (pimo) median fluorescence intensity (MFI) after gating on total, live, singlet, and CD45⁺ CD11b⁺ Ly6G⁻ for F4/80⁺ or CD64⁺ macrophages from infected (Inf) and contralateral (Con) ears from the same mouse. (B) Representative flow cytometry histograms showing pimonidazole MFI after gating on F4/80⁺ macrophages from the infected ear or corresponding dLN and spleen of the same mouse. (C) Quantification of pimonidazole MFI in macrophages from the skin, dLN, and spleen at 1 week p.i. (D) Quantification of pimonidazole MFI in macrophages from the skin, dLN, and spleen at 5 weeks p.i. (E) Representative flow cytometry histograms showing pimonidazole MFI after gating on macrophages from infected skin that were Ly6C^{hi} or Ly6C^{lo} at 5 week p.i. (F) Quantification of pimonidazole MFI for Ly6C^{hi} or Ly6C^{lo} macrophages from infected ears from panel E. Fluorescence minus one (FMO) controls for pimonidazole staining are seen in gray (A, B, E). Data (Continued on next page)

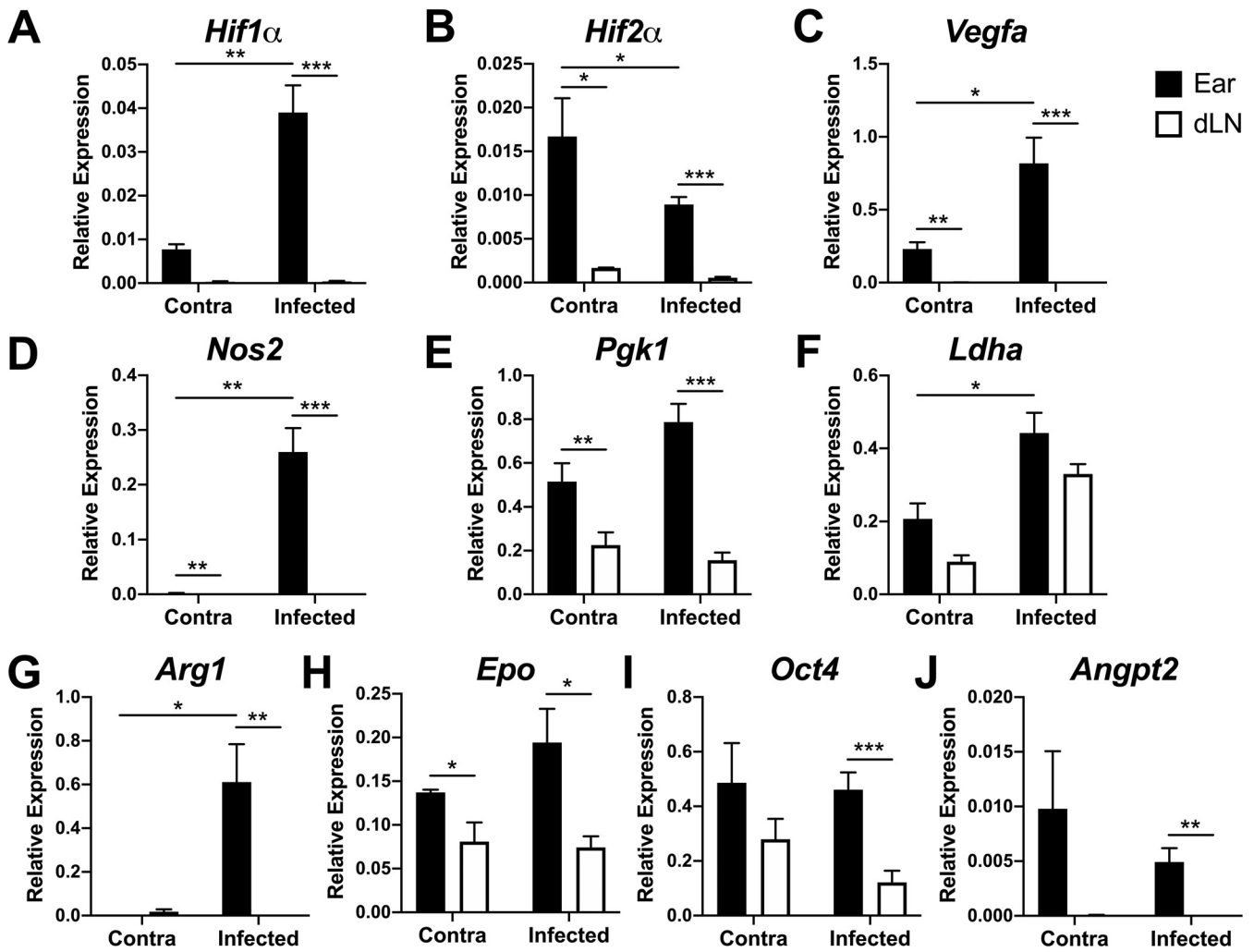


FIG 2 Pan-HIF signaling is preferentially activated at the site of infection following *L. major* inoculation *in vivo*. C57BL/6 mice were infected with 2×10^6 *L. major* parasites intradermally in the ear. At 2 to 4 weeks p.i., infected and contralateral ears and dLNs were digested and mRNA was extracted from total ear cells. The expression of *Hif1α* (A), *Hif2α* (B), *Vegfa* (C), *Nos2* (D), *Pdgk1* (E), *Ldha* (F), *Arg1* (G), *Epo* (H), *Oct4* (I), and *Angpt2* (J) was analyzed by quantitative real-time PCR. Relative mRNA expression normalized to the housekeeping gene *Rps11* is presented as the mean + SEM. Results shown here are from 1 representative experiment of 3 individual experiments that included 3 to 9 mice per group. *, $P \leq 0.05$; **, $P < 0.01$; ***, $P < 0.001$, *t* test comparing ears to dLNs.

Given that macrophages experience hypoxic conditions and HIF and VEGF-A are elevated at the site of infection in the ear compared to other sites of immune activation, such as the dLNs, we examined the expression of other HIF-target genes at the site of infection. Furthermore, to identify the HIF pathway activated during *L. major* infection, we investigated the expression of HIF-1 α -specific (*Nos2*, *Pdgk1*, and *Ldha*) and HIF-2 α -specific (*Arg1*, *Epo*, *Oct4*, and *Angpt2*) target genes. As with *Vegfa*, the expression of HIF-1 α -specific targets *Nos2* and *Pdgk1* was significantly higher in the skin than in the dLN, independent of the infection status of the ear (Fig. 2D and E). However, *Ldha* expression did not differ significantly between the ears and dLNs (Fig. 2F). The expression of HIF-2 α -specific targets *Arg1*, *Epo*, *Oct4*, and *Angpt2* was significantly higher in infected skin compared to the corresponding dLN (Fig. 2G to J). It should be noted that many HIF-2 α -specific targets (*Epo*, *Oct4*, and *Angpt2*) were elevated in contralateral

FIG 1 Legend (Continued)

shown were pooled from 2 experiments with 5 mice per group per time point ($n=10$ mice per condition). Data are presented as the mean plus standard error of the mean (SEM). **, $P < 0.01$; ***, $P < 0.001$, paired *t* test comparing macrophages from infected skin to dLNs or spleens or comparing dermal macrophages with variable Ly6C expression.

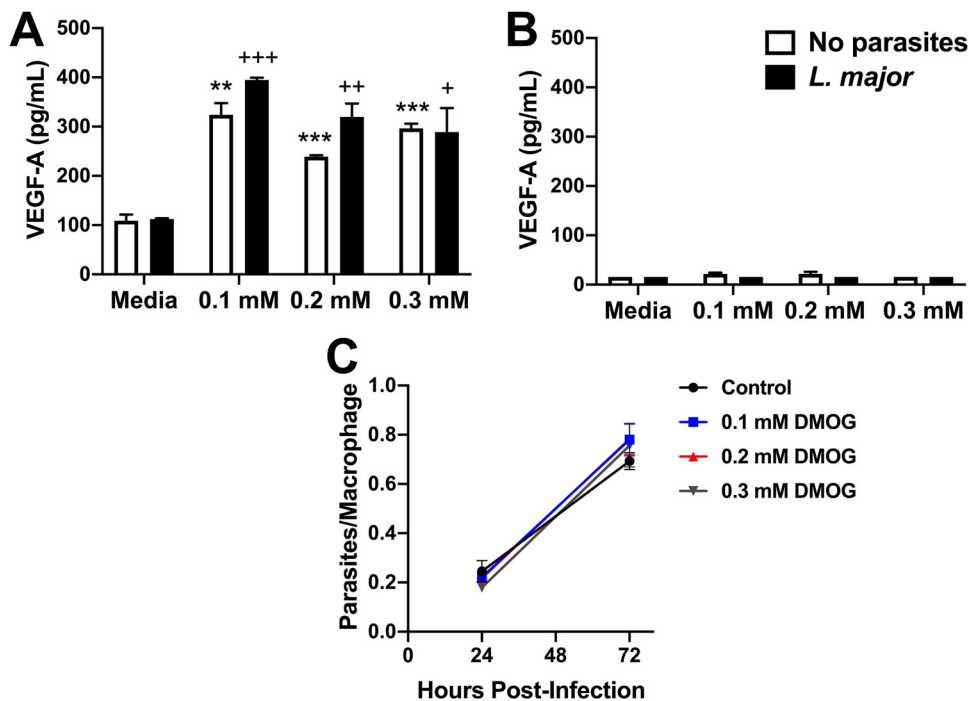


FIG 3 HIF stabilization does not restrict parasite growth during *L. major* infection. Bone marrow-derived macrophages (BMDMs) were infected with *L. major* parasites for 2 h, extracellular parasites were washed away, and cells were exposed to dimethylxalylglycine (DMOG) at various concentrations (0.1 mM, 0.2 mM, or 0.3 mM) for 24 to 72 h in triplicate. (A and B) VEGF-A production was measured with ELISA in BMDMs derived from *LysM^{Cre} ARNT^{f/+}* mice (A) and *LysM^{Cre} ARNT^{f/f}* mice (B) after 24 h. Results shown are from 1 representative experiment of at least 2 individual experiments. (C) DsRed *L. major* parasite burden in BMDMs quantified by fluorescence microscopy with and without DMOG treatment at 24 and 72 h p.i. Results shown here are pooled from 2 individual experiments. Data are presented as the mean + SEM. **, $P < 0.01$; ***, $P < 0.001$, *t* test comparing DMOG treatment to medium control in uninfected cells; +, $P \leq 0.05$; ++, $P < 0.01$; +++, $P < 0.001$, *t* test comparing DMOG treatment to medium control in infected cells.

ears compared to the corresponding dLN, which is consistent with basal *Hif2 α* expression in uninfamed skin. Taken together, these data suggest that both HIF-1 α and HIF-2 α are activated at the site of *L. major* infection.

We previously reported that macrophages are the major cell type in the lesions that express *Hif1 α* and the HIF target gene *Vegfa* (12). We also showed that increased VEGF-A expression is dependent on myeloid ARNT/HIF signaling during *L. major* infection (12). Therefore, we aimed to develop an *in vitro* system that mimics HIF activation *in vivo* to determine if HIF activation in macrophages limits parasite numbers. To mimic macrophage HIF activation, bone marrow-derived macrophages (BMDM) were infected with DsRed fluorescent *L. major* parasites and exposed to dimethylxalylglycine (DMOG), an HIF-stabilizing agent, *in vitro*. To confirm that DMOG stabilizes HIF, leading to HIF activation during infection, VEGF-A production was measured by enzyme-linked immunosorbent assay (ELISA). DMOG exposure at various concentrations (0.1 mM, 0.2 mM, and 0.3 mM) for 24 h induced VEGF-A production from uninfected and *L. major*-infected macrophages (Fig. 3A). Furthermore, ARNT is the constitutive binding partner of the HIF-1 α and HIF-2 α subunits, and ARNT deficiency is an approach to study pan-HIF inhibition (23). Therefore, these experiments were performed in BMDMs generated from *LysM^{Cre} ARNT^{f/f}* mice, which are deficient in myeloid ARNT/HIF signaling, and *LysM^{Cre} ARNT^{f/+}* control mice. Using these genetic mouse models demonstrates DMOG treatment is directly affecting ARNT/HIF signaling, and not acting as an off-target effect. We found DMOG-induced VEGF-A production depended on ARNT/HIF signaling because macrophages derived from *LysM^{Cre} ARNT^{f/f}* mice exhibited impaired VEGF-A production compared to *LysM^{Cre} ARNT^{f/+}* macrophages, independent of

infection status (Fig. 3B; comparing Fig. 3A and B experiments, which were performed at the same time). Next, *L. major* parasite burden in BMDMs was quantified by microscopy following DMOG treatment. Our findings show that HIF stabilization did not alter *L. major* parasite burden in BMDMs at 24 or 72 h postinfection (p.i.) (Fig. 3C). Altogether, these data demonstrate that macrophage HIF activation alone does not modulate parasite growth *in vitro*.

To determine the downstream consequence of ARNT/HIF signaling in macrophages during leishmaniasis, mice exhibiting ARNT deficiency in a myeloid-specific manner were infected with *L. major*. Confirming previous results, we found that $\text{LysM}^{\text{Cre}} \text{ARNT}^{\text{f/f}}$ mice develop significantly larger lesions following *L. major* infection than $\text{LysM}^{\text{Cre}} \text{ARNT}^{\text{f/+}}$ mice, with no difference in parasite burden between groups (Fig. 4A and B) (12). Infected $\text{LysM}^{\text{Cre}} \text{ARNT}^{\text{f/f}}$ mice showed enhanced immunopathology with more CD4^+ T cells at the site of infection, compared to $\text{LysM}^{\text{Cre}} \text{ARNT}^{\text{f/+}}$ control mice, at 3.5 to 5 weeks p.i. (Fig. 4C) when lesions are at their peak size and clearly differ between $\text{LysM}^{\text{Cre}} \text{ARNT}^{\text{f/f}}$ and $\text{LysM}^{\text{Cre}} \text{ARNT}^{\text{f/+}}$ mice (Fig. 4A).

Because the CD4^+ T cell response predominantly develops in the dLNs, we evaluated lymph node hypertrophy following *L. major* infection. Mice deficient in myeloid ARNT/HIF signaling presented with more total immune cells in the dLN and more CD45^+ hematopoietic immune cells compared to controls (Fig. 4D and E). Next, we investigated the quality and quantity of the Th1 immune response in dLNs of infected $\text{LysM}^{\text{Cre}} \text{ARNT}^{\text{f/f}}$ and $\text{LysM}^{\text{Cre}} \text{ARNT}^{\text{f/+}}$ mice using CD44 as a marker of T cell activation. Following infection, mice deficient in myeloid ARNT/HIF signaling had a higher percentage and number of proliferating CD44^+ CD4^+ T cells compared to control mice as assessed by BrdU incorporation coupled with flow cytometry (Fig. 4F and G). In addition, $\text{LysM}^{\text{Cre}} \text{ARNT}^{\text{f/f}}$ mice exhibited a greater percentage and number of IFN- γ -producing CD44^+ CD4^+ T cells compared to $\text{LysM}^{\text{Cre}} \text{ARNT}^{\text{f/+}}$ mice after *L. major* infection (Fig. 4H and I). Similar to IFN- γ production, $\text{LysM}^{\text{Cre}} \text{ARNT}^{\text{f/f}}$ mice also had a higher percentage and number of tumor necrosis factor α (TNF- α)-producing CD44^+ CD4^+ T cells compared to $\text{LysM}^{\text{Cre}} \text{ARNT}^{\text{f/+}}$ mice following infection (Fig. 4J and K).

Given that CD8^+ T cells can also contribute to parasite control and disease severity during *Leishmania* infection, activated CD8^+ T cells from the dLN were investigated by flow cytometry. We found that mice deficient in myeloid ARNT/HIF signaling had a higher number of proliferating CD44^+ CD8^+ T cells than controls, despite there was no significant difference in the percentage of BrdU $^+$ CD44^+ CD8^+ T cells between groups during infection (Fig. 4L and M). Unlike findings for CD44^+ CD4^+ T cells, there were no significant differences in IFN- γ or TNF- α -producing CD44^+ CD8^+ T cells from dLNs between infected $\text{LysM}^{\text{Cre}} \text{ARNT}^{\text{f/f}}$ and $\text{LysM}^{\text{Cre}} \text{ARNT}^{\text{f/+}}$ mice (Fig. 4N to Q). Taken together, these results suggest the increased lesion sizes in $\text{LysM}^{\text{Cre}} \text{ARNT}^{\text{f/f}}$ mice are associated with enhanced immunopathology characterized by a heightened CD4^+ Th1 cell response during *L. major* infection.

Because macrophage ARNT/HIF signaling contributes to elevated VEGF-A expression during *L. major* infection and VEGFR-A/VEGFR-2 signaling leads to lymphangiogenesis, we hypothesized that ARNT/HIF signaling in myeloid cells promotes lymphangiogenesis, which decreases immunopathology. To test this hypothesis, $\text{LysM}^{\text{Cre}} \text{ARNT}^{\text{f/f}}$ and $\text{LysM}^{\text{Cre}} \text{ARNT}^{\text{f/+}}$ mice were infected with *L. major*. Histologically, ears from $\text{LysM}^{\text{Cre}} \text{ARNT}^{\text{f/f}}$ mice contained a cellular infiltrate that exceeded that of $\text{LysM}^{\text{Cre}} \text{ARNT}^{\text{f/+}}$ control animals (Fig. 5A and B). To specifically examine the lymphatic vasculature, ears were stained with lymphatic vessel endothelial receptor 1 (LYVE-1) and images at 2 different magnifications were acquired with immunofluorescence microscopy (Fig. 5C to F). For the analysis of LYVE-1, the tissue area was normalized between groups while investigating lymphatic vessel density to control for the enhanced inflammation in infected $\text{LysM}^{\text{Cre}} \text{ARNT}^{\text{f/f}}$ mice. We found mice deficient in myeloid ARNT/HIF signaling exhibited a significant decrease in the percentage of tissue staining for LYVE-1 compared to $\text{LysM}^{\text{Cre}} \text{ARNT}^{\text{f/+}}$ mice following infection (Fig. 5G). Moreover, infected $\text{LysM}^{\text{Cre}} \text{ARNT}^{\text{f/f}}$ mice presented with a significant decrease in the density of lymphatic vessels at the site of infection compared to LysM^{Cre}

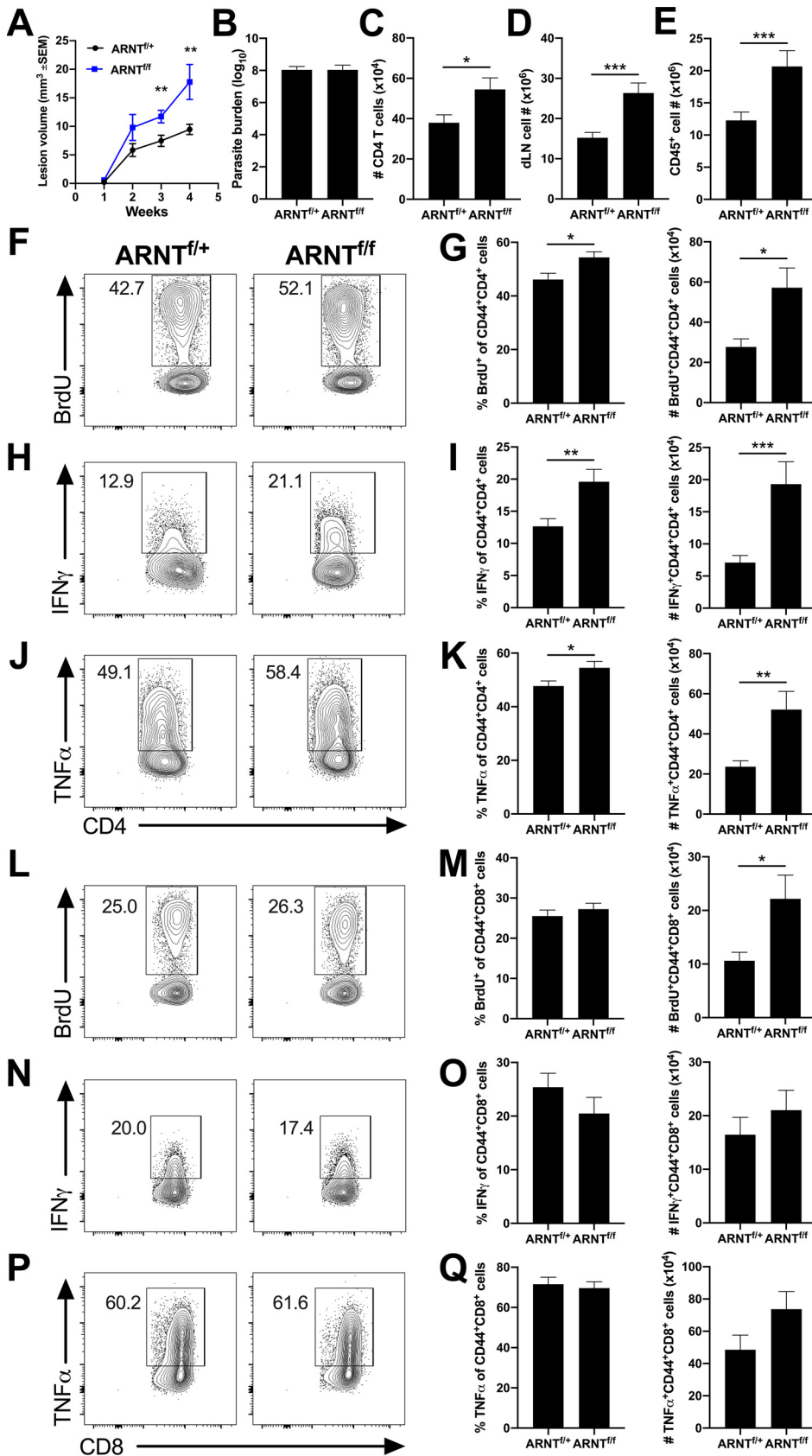


FIG 4 Exacerbated inflammation in mice lacking myeloid pan-HIF signaling is associated with a heightened Th1 immune response during *L. major* infection. LysM^{Cre} ARNT^{fl/fl} or LysM^{Cre} ARNT^{fl/+} mice were infected with (Continued on next page)

ARNT^{f/+} controls (Fig. 5H). Of note, uninflamed contralateral ears from infected LysM^{Cre} ARNT^{f/+} and LysM^{Cre} ARNT^{f/f} mice did not differ in their lymphatic vessel density (data not shown). Parasite burdens in the ear are not different between infected LysM^{Cre} ARNT^{f/+} and LysM^{Cre} ARNT^{f/f} mice (Fig. 4B) (12). Given the enhanced dLN CD4⁺ Th1 response and the defective lymphangiogenesis in the ear, we investigated parasite loads in the dLN. Similar to the ear, at 4 weeks p.i. there was no detectable difference in parasite burdens between infected LysM^{Cre} ARNT^{f/+} and LysM^{Cre} ARNT^{f/f} mice, as assessed by limiting dilution assay (LDA) on dLNs or real-time PCR (data not shown). Taken together, these data suggest that myeloid ARNT/HIF signaling mediates lymphangiogenesis during *L. major* infection, and that inhibiting this pathway exacerbates pathology, demonstrating a tissue-protective role for the ARNT/HIF/VEGF-A/VEGFR-2 signaling pathway during infection-induced inflammation.

DISCUSSION

A general feature of inflammation is hypoxia (16), which is defined as having an inadequate oxygen supply and is often due to a heightened demand for oxygen in tissues (24). Several factors contribute to the need for oxygen in inflamed tissues, including increased cell recruitment, cell proliferation, shifts in cellular metabolism, and parasite proliferation and metabolism in the case of leishmaniasis. Hypoxia is a characteristic of many inflammatory diseases, including inflammatory bowel disease, herpes stromal keratitis, obesity, rheumatoid arthritis, and tuberculosis (24–27). Furthermore, increased inflammatory hypoxia specifically in the myeloid cell compartment has been associated with more severe pathology in clinical disease (26). Similar to other inflammatory diseases, cutaneous lesions resulting from *Leishmania* infection exhibit hypoxia alongside a large myeloid cell infiltration (14). Under normal conditions, regions of the epidermis and dermis exhibit physiologic hypoxia with 0.5% to 5% O₂ (1% = 1.013 kPa), depending on the site and proximity to oxygenated vasculature (24, 28–31). During development, the low-oxygen tension in the skin is critical for keratinocyte differentiation and epidermal barrier function (32), but sustained post-natal hypoxia of the skin is thought to result from distance from the lung, the site of blood oxygenation (24). Following *L. major* footpad infection, the inflamed footpad exhibits 2.8% O₂ compared to the contralateral footpad at 5.2% O₂ (14). In this study, we detected macrophages in the skin staining for pimonidazole, suggesting that

FIG 4 Legend (Continued)

2 × 10⁶ *L. major* metacyclic parasites intradermally in the ear. Immune cell populations were analyzed at 3.5 to 5 weeks postinfection (p.i.) when lesions developed. (A) Lesion volume was monitored weekly. (B) Parasite burdens were determined at 4 weeks p.i. by limiting dilution assay. Lesion and parasite count data were pooled from 2 independent experiments with 11 to 24 mice per group. (C) Infected ears were processed, and total cell numbers were counted. Cells were stained and analyzed by flow cytometry and the total number of CD4⁺ T cells was calculated. Dermal CD4⁺ T cell data shown here were pooled from 3 independent experiments (total of 29 LysM^{Cre} ARNT^{f/+} and 24 LysM^{Cre} ARNT^{f/f} mice). (D to Q) The dLN of infected ears is the source of cells analyzed for T cell proliferation and cytokine production. dLN cells were treated with BFA/monensin and PMA/ionomycin for 4 h before surface and intracellular staining. (D) dLNs draining infected ears were processed and total cell numbers were counted. (E) Cells were analyzed by flow cytometry and the total number of CD45⁺ cells was calculated. dLN and CD45⁺ cell number data shown here were pooled from 3 independent experiments (total of 29 LysM^{Cre} ARNT^{f/+} and 22 LysM^{Cre} ARNT^{f/f} mice). (F) Representative flow cytometry plots showing BrdU of CD4⁺ CD44⁺ T cells. (G) Quantification of percentage and number of BrdU⁺ cells of CD4⁺ CD44⁺ T cells. (H) Representative flow cytometry plots showing IFN-γ of CD4⁺ CD44⁺ T cells. (I) Quantification of percentage and number of IFN-γ⁺ cells of CD4⁺ CD44⁺ T cells. (J) Representative flow cytometry plots showing TNF-α of CD4⁺ CD44⁺ T cells. (K) Quantification of percentage and number of TNF-α⁺ cells of CD4⁺ CD44⁺ T cells. (L) Representative flow cytometry plots showing BrdU of CD8⁺ CD44⁺ T cells. (M) Quantification of percentage and number of BrdU⁺ cells of CD8⁺ CD44⁺ T cells. (N) Representative flow cytometry plots showing IFN-γ of CD8⁺ CD44⁺ T cells. (O) Quantification of percentage and number of IFN-γ⁺ cells of CD8⁺ CD44⁺ T cells. (P) Representative flow cytometry plots showing TNF-α on CD8⁺ CD44⁺ T cells. (Q) Quantification of percentage and number of TNF-α⁺ cells of CD8⁺ CD44⁺ T cells. All cells were pregated on total, live, singlet CD45⁺ cells. BrdU proliferation data shown here were pooled from 2 independent experiments (total of 11 LysM^{Cre} ARNT^{f/+} and 13 LysM^{Cre} ARNT^{f/f} mice). Intracellular cytokine data were pooled from 3 independent experiments for IFN-γ (total of 29 LysM^{Cre} ARNT^{f/+} and 22 LysM^{Cre} ARNT^{f/f} mice) and from 2 independent experiments for TNF-α (total of 23 LysM^{Cre} ARNT^{f/+} and 16 LysM^{Cre} ARNT^{f/f} mice). Data are presented as the mean + SEM. *, P ≤ 0.05; **, P < 0.01; ***, P < 0.001, unpaired *t* test comparing infected LysM^{Cre} ARNT^{f/f} mice to infected LysM^{Cre} ARNT^{f/+} controls.

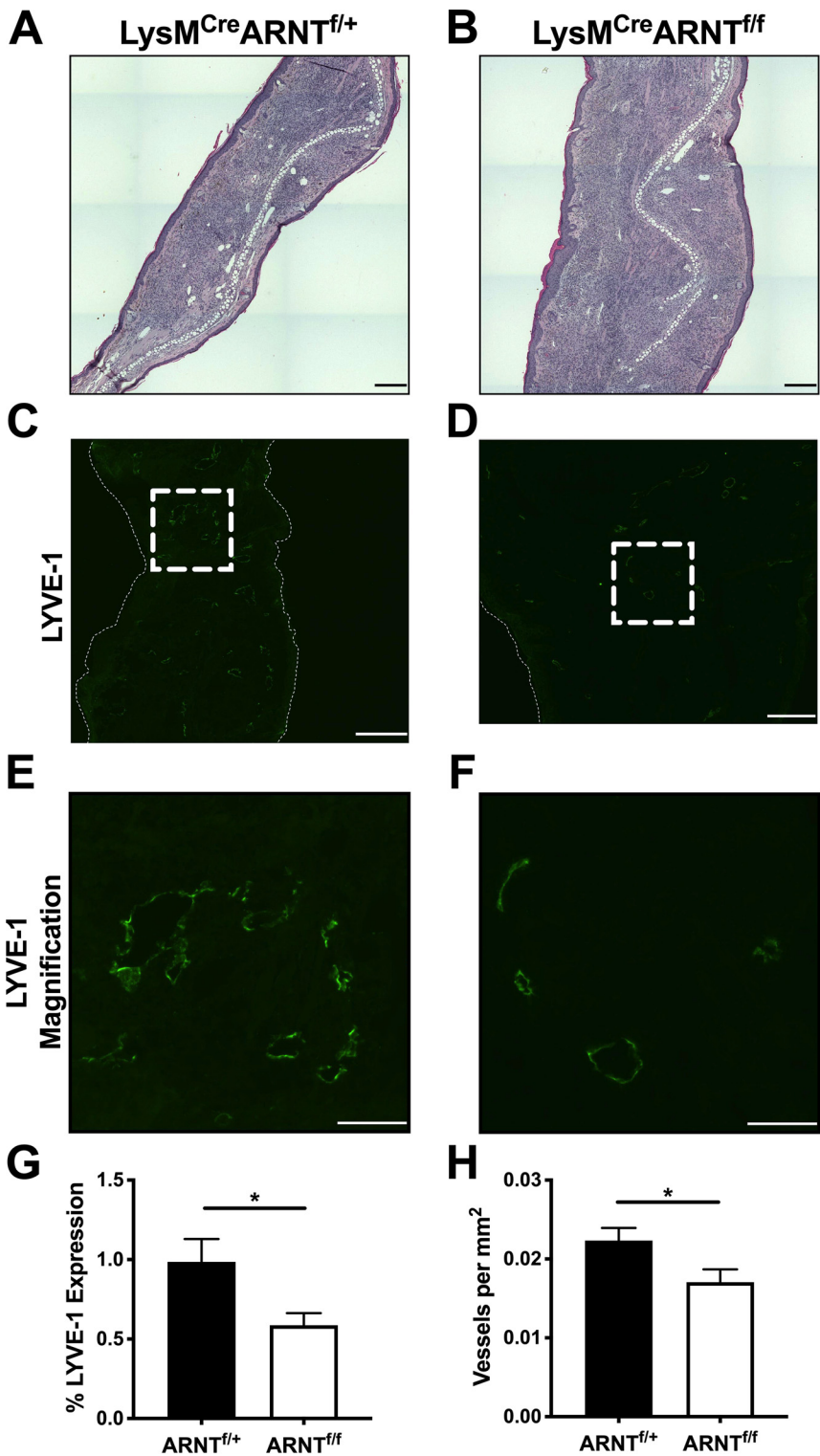


FIG 5 Myeloid pan-HIF signaling promotes lymphangiogenesis during *L. major* infection. $LysM^{Cre} ARNT^{f/f}$ or $LysM^{Cre} ARNT^{f/+}$ mice were infected with 2×10^6 *L. major* metacyclic parasites intradermally in the ear. Ears were analyzed at 4 weeks p.i. (A and B) H&E-stained infected $LysM^{Cre} ARNT^{f/+}$ and $LysM^{Cre} ARNT^{f/f}$ ears. (C and D) Infected $LysM^{Cre} ARNT^{f/+}$ and $LysM^{Cre} ARNT^{f/f}$ ears were stained for LYVE-1 to delineate lymphatic ECs and lymphatic vessels by immunofluorescence microscopy. (E and F) Magnified view of LYVE-1⁺ lymphatic vessels from images C and D. (G) LYVE-1 expression was quantified by immunofluorescence microscopy. (H) Lymphatic vessel density was quantified by microscopy. *, $P \leq 0.05$, *t* test comparing infected $LysM^{Cre} ARNT^{f/f}$ mice to infected $LysM^{Cre} ARNT^{f/+}$ controls. Data are presented as mean + SEM. The data presented were from 2 pooled experiments with a combined total of 8 mice per group. Scale bars: 300 μ m (C and D) and 100 μ m (E and F).

resident skin cells experience hypoxic conditions of $\leq 1.3\%$ O_2 , the percent O_2 where pimonidazole is activated to form covalent adducts with thiol groups in proteins (33). Overall, the skin exists basally in a mildly hypoxic state compared to other organs, and increased inflammatory cell recruitment and proliferation can exacerbate hypoxia in an already hypoxic environment.

Even though hypoxia has been documented following *L. major* infection at the tissue level, we wanted to determine if macrophages in the dermal tissue experience hypoxic conditions, as factors such as proximity to oxygenated blood vessels or length of time in the inflamed tissue may influence the hypoxic signature of an individual cell. For the first time, we found skin macrophages displayed an enhanced hypoxic signature, as measured by pimonidazole staining compared to macrophages in lymphoid organs, and this hypoxia profile directly mirrored the expression of HIF- α target genes. Even though the skin is mildly hypoxic basally, we were surprised to detect similar levels of hypoxia in skin macrophages between inflamed and uninflamed contralateral ears. Upon deeper examination, we found that macrophages expressing the inflammatory monocyte marker Ly6C, suggesting they were recently derived from recruited monocytes (9), exhibited a decreased hypoxic profile compared to resident cells. These data show for the first time that monocyte-derived Ly6C^{hi} macrophages are less hypoxic than resident Ly6C^{lo} macrophages in the skin during cutaneous leishmaniasis, even though both cell types exist in the same microenvironment. Therefore, these data suggest there is heterogeneity in the macrophage population with respect to the longevity within the tissue, and we speculate the oxygenated environment of the blood imprints a metabolic signature that is lost upon entry into inflamed tissues. In addition to proximity to a blood vessel, which contributes to the hypoxic status of cells (34), the amount of time a cell spends in a hypoxic microenvironment may also impact its metabolism and function. Given hypoxic conditions induce a glycolytic profile in macrophages and this metabolic shift can dictate their functionality (35), future studies will be required to characterize how cells are influenced by their tissue microenvironments as they migrate from normoxic vessels into sites of inflammation characterized by chronic hypoxia. Additionally, future work will examine the length of time cells must spend in the tissue for their genomic and metabolic signatures to be reprogrammed. Altogether, these results offer insights into how cells change once they enter a tissue, which is important given their microenvironment can affect their functionality, and thus their ability to control pathogens.

Once established, hypoxia leads to the accumulation and stabilization of HIF- α isoforms. There are 3 HIF- α isoforms, i.e., HIF-1 α , HIF-2 α , and HIF-3 α . While not much is known about HIF-3 α in general, the 2 primary isoforms are HIF-1 α and HIF-2 α . Upon activation, the HIF- α subunit binds to ARNT (HIF-1 β), which is constitutively expressed (36). The HIF- α /ARNT heterodimer is translocated to the nucleus, where it binds to hypoxia-responsive elements of target genes involved in regulating cell metabolism, especially in response to stress (36). While HIF-1 α and HIF-2 α share 48% amino acid sequence homology and induce the expression of many of the same target genes, such as *Vegfa*, each HIF- α subunit also regulates a distinct subset of genes (37, 38). Consistent with leishmanial lesions being hypoxic, HIF-1 α is elevated in lesions from infected humans and mice (12, 18, 19, 21, 39); however, the expression of HIF-2 α has not been examined in this context. In addition to HIF-1 α , we show for the first time that HIF-2 α and HIF-2 α target genes are expressed preferentially in the skin during *L. major* infection. Given that myeloid *Arnt* deletion affects both HIF-1 α and HIF-2 α signaling (23), we investigated the expression of target genes specific to each isoform. We found evidence that both HIF-1 α and HIF-2 α target genes were elevated during *L. major* infection, suggesting both HIF-1 α and HIF-2 α signaling are active in cutaneous leishmaniasis. When cutaneous inflammatory lesions were at their peak lesion size, the HIF-1 α targets *Nos2* and *Pgk1* were expressed at higher levels in the inflamed skin than in the corresponding dLN. Similarly, HIF-2 α targets *Arg1*, *Epo*, *Oct4*, and *Angpt2* were expressed at higher levels in the inflamed skin than in the corresponding dLN. While

myeloid HIF-1 α plays a role in parasite killing through NO production during *L. major* infection (19), the downstream consequence of HIF-2 α signaling in any cell type during leishmaniasis is unknown. Here, we found HIF-2 α was expressed in both uninflamed and inflamed skin, supporting our observation that many HIF-2 α target genes were expressed in the skin regardless of the inflammatory status. Altogether, these data suggest both HIF- α pathways are active and may contribute to pathogen control and/or clinical disease. Future work using transgenic mouse models for deletion of HIF-1 α and HIF-2 α individually will be required to distinguish the relevance of each HIF- α pathway in the pathogenesis of cutaneous leishmaniasis, as well as other pathological diseases.

While the immense recruitment of myeloid cells is critical for parasite control, the continuous recruitment of inflammatory cells into the skin must be restricted to prevent immunopathology and maintain tissue integrity. To limit immunopathology during cutaneous leishmaniasis, we speculate lymphangiogenesis occurs to provide an exit route for recruited cells and excess fluid back to the circulation (21). During leishmaniasis, lymphangiogenesis is mediated by VEGF-A binding to the corresponding receptor VEGFR-2 on lymphatic endothelial cells (ECs) (21). In this work, we build upon our previous findings and show that macrophage ARNT/HIF/VEGF-A leads to lymphangiogenesis and lesion resolution during *L. major* infection. In the absence of myeloid ARNT/HIF- α signaling, infected mice displayed exacerbated immunopathology characterized by increased numbers of CD4⁺ T cells in the skin and an enhanced overall immune response, as evidenced by larger dLN hypertrophy in infected LysM^{Cre} ARNT^{ff} mice than in controls. While we have previously reported increased numbers of inflammatory monocytes are associated with immunopathology in LysM^{Cre} ARNT^{ff} mice (12), this is the first time elevated numbers of CD4⁺ T cells have been detected in these mice following *L. major* infection. In general, infected LysM^{Cre} ARNT^{ff} mice exhibited an enhanced CD4⁺ T cell response, with larger percentages and numbers of proliferating, IFN- γ -producing, and TNF- α -producing CD4⁺ T cells compared to LysM^{Cre} ARNT^{f/+} controls. Surprisingly, the enhanced CD4⁺ T cell response did not result in lower parasite numbers in LysM^{Cre} ARNT^{ff} mice. Even though we detected more CD4⁺ T cells producing IFN- γ , which would suggest better parasite control, we speculate parasite load is not decreased due to a defect in Nos2 expression by LysM^{Cre} ARNT^{ff} macrophages (12). Supporting this hypothesis, the addition of IFN- γ to macrophages lacking HIF-1 α does not lead to optimal control of parasitic or bacterial infections due to insufficient NO production (19, 40). Therefore, even though T cells are producing more IFN- γ in infected LysM^{Cre} ARNT^{ff} mice, HIF- α deficient macrophages cannot optimally respond to control *Leishmania* parasites. HIF-1 α -deficient macrophages also fail to suppress T cell proliferation and function under hypoxia, suggesting macrophage HIF-1 α suppresses T cell responses in tumors, which is consistent with our findings during infection (41). In addition to IFN- γ , there was also a higher percentage and number of CD4⁺ T cells producing TNF- α in infected LysM^{Cre} ARNT^{ff} mice, which would also suggest lower parasite numbers. However, T cells are not the only source of TNF- α , and other cellular sources may produce sufficient TNF- α to kill parasites. Given macrophage TNF- α production is intact in infected LysM^{Cre} ARNT^{ff} mice, we hypothesize T cell-derived TNF- α does not enhance parasite control in the skin when macrophage TNF- α is sufficient (12).

Given infected LysM^{Cre} ARNT^{ff} mice did not exhibit a compromised immune response, we speculate that the preexisting lymphatics, which are present prior to infection, are sufficient and capable of mediating parasite or dendritic cell migration from the site of infection to the dLN to initiate CD4⁺ Th1 response. In this mouse model, dLN T cell activation occurs by day 7 p.i. but lymphatic EC proliferation does not peak until 21 days p.i., suggesting the expansion of the lymphatics follows T cell priming and the accumulation of inflammatory cells in the skin, which markedly increase at 14 days p.i. Therefore, we propose lymphangiogenesis only occurs after accumulation of inflammatory cells in the lesion, and thus defects in lymphangiogenesis in the infected LysM^{Cre} ARNT^{ff} mice would not impact initial T cell activation. Our data show lymphangiogenesis is required to orchestrate inflammatory cell exit from the dermal tissue to allow for lesion

resolution. Without myeloid ARNT/HIF-mediated lymphangiogenesis, the recruited cells, such as inflammatory monocytes and CD4⁺ T cells, extravasated fluid, and inflammatory mediators such as cytokines and chemokines are sequestered at the site of infection, leading to larger lesions and impaired wound healing. Others have reported a role for lymphangiogenesis in viral dissemination and tumor metastasis (42, 43). We did not detect increased parasite loads in the dLN when lymphangiogenesis was optimal, suggesting the expanded lymphatics are not a major contributor to parasite dissemination after lesions are established. Given parasites are detected in the dLN, these data suggest the preexisting lymphatics are sufficient for parasite dissemination to the dLN. However, this remains an important unanswered question for other *Leishmania* species resulting in cutaneous leishmaniasis that are more associated with dissemination, such as *Leishmania braziliensis*.

Our findings show that the absence of the ARNT/HIF pathway in myeloid cells does not compromise the immune response because parasite burdens were similar in LysM^{Cre} ARNT^{fl/fl} and control mice. While others demonstrated that HIF stabilization decreases bacterial and fungal burdens within macrophages (40, 44), *Leishmania* parasite growth was not affected by HIF stabilization alone. HIF can be stabilized by two dominant mechanisms: (i) inhibiting prolyl hydroxylase (PHD) enzymes or (ii) factor inhibiting HIF (FIH) (45). Earlier studies with *L. major* examined the effects of HIF stabilization by inhibiting PHD enzymes without affecting FIH (19); however, it is not known if PHD enzymes or FIH stabilizes HIF *in vivo* during infection. Here, we stabilized HIF using DMOG, which inhibits both PHD enzymes and FIH, and found HIF stabilization does not impact parasite growth or lead to parasite killing. Therefore, we hypothesize that multiple signals from the microenvironment are required for parasite killing. For instance, hypoxia in combination with proinflammatory cytokines leads to HIF-1 α -mediated anti-leishmanial immunity in macrophages, but HIF-1 α accumulation alone does not yield the same effect (19). Here, we showed that myeloid ARNT/HIF signaling promotes VEGF-A-mediated lymphangiogenesis during cutaneous leishmaniasis to restrict tissue inflammation. Considered alongside elegant work from others, our results suggest dermal macrophages play dual roles in hypoxic tissue by participating in pathogen control and orchestrating lymphatic remodeling to limit immunopathology during leishmaniasis.

MATERIALS AND METHODS

Mice. Female C57BL/6NCR mice were purchased from the National Cancer Institute. To achieve myeloid-specific *Arnt* conditional-knockout mice, mice expressing the LysM^{Cre} allele were crossed with mice with a floxed *Arnt* conditional allele, as previously described (23, 46). Therefore, all mice, including controls, were homozygous for the LysM^{Cre} allele. The LysM^{Cre} ARNT^{fl/fl} and LysM^{Cre} ARNT^{fl/+} control mice were a gift from M. Celeste Simon (University of Pennsylvania, Philadelphia, PA). For infections, LysM^{Cre} ARNT^{fl/fl} mice were infected alongside LysM^{Cre} ARNT^{fl/+} controls. Mice were housed under pathogen-free conditions at the University of Arkansas for Medical Sciences (UAMS) and used for experiments at 6 to 8 weeks of age. All procedures were approved by the UAMS IACUC and performed in accordance with institutional guidelines.

Parasites. *Leishmania major* (WHO/MHOM/IL/80/Friedlin) and DsRed fluorescent *L. major* Friedlin strain parasites were grown *in vitro* in Schneider's Drosophila medium (Gibco) supplemented with 20% heat-inactivated fetal bovine serum (FBS, Invitrogen), 2 mM L-glutamine (Sigma), 100 U/ml penicillin, and 100 μ g/ml streptomycin (Sigma). Metacyclic stationary-phase promastigotes were isolated from 4- to 5-day-old cultures by Ficoll density gradient separation (Sigma) (47).

In vivo infections. For infections, 10 μ l of phosphate-buffered saline (PBS) (Gibco) containing 2×10^6 parasites was injected intradermally into the ear. Only one ear of each mouse was infected and the other contralateral ear of the same mouse, which was not infected or injected, served as an uninfected control. Ear thickness and lesion area were monitored weekly with a caliper, and lesion volume was calculated. Ears were digested enzymatically for 90 min at 37°C in 0.25 mg/ml liberase (Roche) with 10 μ g/ml DNase I (Sigma) in incomplete RPMI 1640 medium (Gibco). Limiting dilution assays were performed to determine parasite burdens in the tissue (48).

Flow cytometry. For flow cytometric analysis of dermal cells from the ears, cells were surface stained after enzymatic digestion and processing. For draining lymph node (dLN) flow cytometric analysis, cells were stimulated with brefeldin A (BFA; 1:1,000; eBioscience), monensin (1:1,000; eBioscience), PMA (100 ng/ml; Abcam), and ionomycin (1 μ g/ml; Sigma) for 4 h before viability and surface staining. To determine cell viability, cells were incubated with fixable Aqua dye (Invitrogen). Fc receptors were blocked with 2.4G2 anti-mouse CD16/32 (Invitrogen or BioXCell) and 0.2% normal rat IgG (BioXCell).

Cells were surface stained using α -CD45 AF700 (eBiosciences), as well as α -CD4 BV605 (Biolegend), α -CD8 β PerCpCy5.5 (Biolegend), α -CD64 PECy7, (Biolegend), α -CD64 BV711, (Biolegend), α -CD11b BV605 (Biolegend), and α -Ly6C PerCpCy5.5 (eBiosciences) in the presence of brilliant violet buffer (BD Biosciences). Intracellular cytokine staining was performed using the Foxp3 intracellular staining kit (Life Technologies) or the BrdU kit (BD Pharmingen) combined with α -CD3 APCeF780 (eBiosciences), α -IFN- γ PECy7 (eBiosciences), and α -TNF- α PE (eBiosciences). For flow cytometry, cell events were acquired on an LSRII Fortessa flow cytometer (BD Biosciences) and analyzed using FlowJo (Tree Star).

BrdU incorporation. BrdU (BD Pharmingen, 0.8 mg/ml) was administered in drinking water for 3 days, and mice were injected intraperitoneally (i.p.) with 1 mg BrdU in 100 μ l at 24 h and 1 h before euthanasia. After cell-surface staining, cells were fixed, permeabilized, and treated with DNase I using the BrdU staining kit (BD Pharmingen). Intracellular staining was performed with α -BrdU-FITC according to the manufacturer's instructions.

Pimonidazole. To determine hypoxia at the cellular level, each infected mouse was injected with 1.5 mg pimonidazole (Hypoxyprobe kit) in 200 μ l PBS i.p. 90 min before sacrifice. After cell-surface staining, cells were fixed and permeabilized using the Foxp3 intracellular staining kit. Intracellular staining was performed with α -pimonidazole-FITC (1:100) according to the manufacturer's instructions. Fluorescence minus one (FMO) controls for pimonidazole staining are shown in gray in the representative histograms.

mRNA extraction and real-time PCR. mRNA was extracted with the EZNA Total RNA kit I (Omega Bio-tek). RNA was reverse transcribed with the High-Capacity cDNA reverse transcription kit (Applied Biosystems). Quantitative real-time PCR was performed using SYBR green PCR Master Mix and a QuantStudio 6 Flex real-time PCR system (Life Technologies). Mouse primer sequences were selected from the PrimerBank (<http://pga.mgh.harvard.edu/primerbank/>): *Vegfa* (forward 5'-ATCTTCAAGCCGTCCTGTGT-3' and reverse 5'-GCATTCACATCTGCTGTGT-3'), *Hif1 α* (forward 5'-TCCCCTCTCCTGTAAGCAAG-3' and reverse 5'-TCGACGTTCCAGAACTCATCT-3'), *Hif2 α* (forward 5'-CTCCAGGAGCTCAAAGGTG-3' and reverse 5'-CAGGTAAGGCTCGAACGATG-3'), *Nos2* (forward 5'-ATGGAGACTGTCCAGCAAT-3' and reverse 5'-GGCGCAGAACTGAGGGTA-3'), *Epo* (forward 5'-CATCTGCGACAGTCGAGTCTG-3' and reverse 5'-CACAACCCATCGTGACATTTTC-3'), *Ldha* (forward 5'-TGTCTCCAGCAAAGACTACTGT-3' and reverse 5'-GACTGTACTTGACAATGTTGGGA-3'), *Pgk1* (forward 5'-ATGTCGCTTAACAAGCTG-3' and reverse 5'-GCTCCATTGTCCAAGCAGAAAT-3'), *Angpt2* (forward 5'-CCTCGACTACGACGACTAGT-3' and reverse 5'-TCTGCACCACA TTCTGTTGGA-3'), *Oct4* (forward 5'-AGAGGATCACCTTGGGGTACA-3' and reverse 5'-CGAAGCGACAGATG GTGGTC-3'), *Arg1* (forward 5'-CTCAAGCCAAAGTCCTTAGAG-3' and reverse 5'-AGGAGCTGCATTAGGG ACATC-3'), and *Rps11* (forward 5'-CGTGACGAAGATGAAGATGC-3' and reverse 5'-GCACATTGAATCGACA GTC-3'). The results were normalized to the housekeeping ribosomal protein S14 gene (*Rps11*) using the comparative threshold cycle method ($2^{-\Delta\Delta CT}$) for relative quantification.

Generation of bone marrow-derived macrophages. Bone marrow-derived macrophages (BMDM) were cultured in Dulbecco's modified Eagle medium (DMEM) supplemented with 10% FBS, 2.5% HEPES, 1% antibiotics (pen/strep), and 25% supernatant from L929 cells as a source of macrophage colony-stimulating factor (M-CSF) for 7 days. For experiments, adherent macrophages were removed after 7 days, counted, and transferred to plates in DMEM to allow for adherence overnight at 37°C before *in vitro* infection or stimulation.

***In vitro* infections and microscopy for parasite quantification.** BMDM (250,000 cells per well in a 48-well plate) were infected with DsRed fluorescent *L. major* parasites (MOI 5:1) for 2 h at 37°C in DMEM to allow parasite internalization. After 2 h of infection, macrophages were washed 3 times to remove extracellular parasites. Macrophages were then cultured for 24 h to examine protein production in cell-free supernatants. In experiments to stabilize HIF signaling, macrophages were treated with dimethylxylglycine (DMOG; Sigma) at 3 different concentrations (0.1 mM, 0.2 mM, or 0.3 mM) during the infection. Cells were placed in DMOG for the duration of the experiment after extracellular parasites were washed away. At the end of the experiment, cells were fixed with ice-cold methanol for 3 min and washed twice with PBS; nuclei were then stained with DAPI (4',6-diamidino-2-phenylindole). For each well, 5 random images were acquired on a Keyence BZX fluorescence microscope and analyzed with BZ-X800 Imager Analyzer software that allows for parasite and macrophage cell counting. To normalize the data, the number of parasites was divided by the number of macrophages for each field. Experiments were performed in triplicate.

VEGF-A production. VEGF-A protein was quantified in cell-free supernatants using an enzyme-linked immunosorbent assay (ELISA) to detect murine VEGF-A as directed by the manufacturer (R&D Systems).

Histology and immunofluorescence microscopy. Infected ears from LysM^{Cre} ARNT^{fl/fl} and LysM^{Cre} ARNT^{+/+} mice were fixed in 10% buffered formalin and embedded in paraffin. For histology, 4- μ m longitudinal sections were subjected to hematoxylin and eosin (H&E) stain. For immunofluorescence microscopy, ears were frozen in Tissue-Tek OCT (Sakura). Tissue sections were fixed with 3% formaldehyde, blocked with 10% goat serum (Sigma) for 1 h, and stained with rabbit anti-LYVE-1 (AngioBio) overnight, followed by goat anti-rabbit Alexa Fluor 488 secondary antibody (Life Technologies) for 1 h. Sections were mounted with Prolong Gold containing DAPI (Invitrogen). Images were captured using an Invitrogen EVOS FL Auto 2 microscope. Fluorescence images of ear sections were analyzed using Volocity (Quorum Technologies Inc.). The areas to be analyzed were selected using the region of interest (ROI) tool. An ROI was drawn around all of the section excluding: (i) the epidermis (due to nonspecific binding of the secondary antibody) and (ii) folded areas due to increased background brightness relative to flat tissue. Lymphatic vessel density was determined by counting the LYVE-1⁺ vessels within the specified ROI and dividing the number of LYVE-1⁺ vessels by the total area of the ROI. Percent LYVE-1 expression was determined by using the ROI tool to measure the area of LYVE-1⁺ pixels, dividing the area of LYVE-1⁺ pixels by the total area of

the ROI, and multiplying by 100. The threshold of "14" was selected to exclude the background fluorescence and thus only show the LYVE-1⁺ cells. It should be noted vessels appear as rings in the stained tissue sections, and we did not visualize many LYVE-1⁺ cells outside the morphology of the ring, suggesting the majority of the LYVE-1⁺ events in infected ears were ECs that are part of the diameter of the vessel, and not LYVE-1⁺ macrophages.

Statistics. All data were analyzed using GraphPad Prism 7, and $P \leq 0.05$ was considered statistically significant. Statistical significance was calculated using a 2-tailed Student's unpaired or paired *t* test for a single comparison between groups. A Grubbs' test was used to identify and mathematically remove outlier data points.

ACKNOWLEDGMENTS

We thank Martin Cannon, Craig Forrest, Lu Huang, Lin-Xi Li, and Jason Stumhofer for their critical reading of the manuscript.

T.W. was supported by the University of Arkansas for Medical Sciences Center for Microbial Pathogenesis and Host Inflammatory Responses (funded by National Institutes of Health National Institute of General Medical Sciences Centers of Biomedical Research Excellence grant P20-GM103625) and the Oak Ridge Associated Universities (ORAU) 2019 Ralph E. Powe Junior Faculty Enhancement Award. The authors would also like to thank the Donaghey Scholars Program and the George W. Donaghey Foundation for financial support. The funders had no role in study design, data collection and interpretation, or the decision to submit the work for publication.

Experiments were conceived by T.W. and M.C.S. and performed by A.B., H.R., H.W., M.B., G.V., J.S., and T.W. The paper was written by A.B., H.R., and T.W.

REFERENCES

- Alvar J, Velez ID, Bern C, Herrero M, Desjeux P, Cano J, Jannin J, den Boer M, WHO Leishmaniasis Control Team. 2012. Leishmaniasis worldwide and global estimates of its incidence. *PLoS One* 7:e35671. <https://doi.org/10.1371/journal.pone.0035671>.
- Scott P, Novais FO. 2016. Cutaneous leishmaniasis: immune responses in protection and pathogenesis. *Nat Rev Immunol* 16:581–592. <https://doi.org/10.1038/nri.2016.72>.
- Bacellar O, Lessa H, Schriefer A, Machado P, Ribeiro de Jesus A, Dutra WO, Gollob KJ, Carvalho EM. 2002. Up-regulation of Th1-type responses in mucosal leishmaniasis patients. *Infect Immun* 70:6734–6740. <https://doi.org/10.1128/iai.70.12.6734-6740.2002>.
- Bittencourt AL, Barral A. 1991. Evaluation of the histopathological classifications of American cutaneous and mucocutaneous leishmaniasis. *Mem Inst Oswaldo Cruz* 86:51–56. <https://doi.org/10.1590/s0074-02761991000100009>.
- Gonzalez-Lombana C, Gimblet C, Bacellar O, Oliveira WW, Passos S, Carvalho LP, Goldschmidt M, Carvalho EM, Scott P. 2013. IL-17 mediates immunopathology in the absence of IL-10 following *Leishmania major* infection. *PLoS Pathog* 9:e1003243. <https://doi.org/10.1371/journal.ppat.1003243>.
- Oliveira F, Bafica A, Rosato AB, Favali CB, Costa JM, Cafe V, Barral-Netto M, Barral A. 2011. Lesion size correlates with *Leishmania* antigen-stimulated TNF-levels in human cutaneous leishmaniasis. *Am J Trop Med Hyg* 85:70–73. <https://doi.org/10.4269/ajtmh.2011.10-0680>.
- Pereira LO, Moreira RB, de Oliveira MP, Reis SO, de Oliveira Neto MP, Pirmez C. 2017. Is *Leishmania* (*Viannia*) *braziliensis* parasite load associated with disease pathogenesis? *Int J Infect Dis* 57:132–137. <https://doi.org/10.1016/j.ijid.2017.01.036>.
- Terabe M, Kuramochi T, Ito M, Hataba T, Sanjoba C, Chang KP, Onodera T, Matsumoto Y. 2000. CD4(+) cells are indispensable for ulcer development in murine cutaneous leishmaniasis. *Infect Immun* 68:4574–4577. <https://doi.org/10.1128/iai.68.8.4574-4577.2000>.
- Leon B, Lopez-Bravo M, Ardavin C. 2007. Monocyte-derived dendritic cells formed at the infection site control the induction of protective T helper 1 responses against *Leishmania*. *Immunity* 26:519–531. <https://doi.org/10.1016/j.immuni.2007.01.017>.
- Petritis PM, Manzoni-de-Almeida D, Gimblet C, Gonzalez Lombana C, Scott P. 2012. *Leishmania mexicana* induces limited recruitment and activation of monocytes and monocyte-derived dendritic cells early during infection. *PLoS Negl Trop Dis* 6:e1858. <https://doi.org/10.1371/journal.pntd.0001858>.
- Ribeiro-Gomes FL, Peters NC, Debrabant A, Sacks DL. 2012. Efficient capture of infected neutrophils by dendritic cells in the skin inhibits the early anti-leishmania response. *PLoS Pathog* 8:e1002536. <https://doi.org/10.1371/journal.ppat.1002536>.
- Weinkopf T, Roys H, Bowlin A, Scott P. 2019. *Leishmania* infection induces macrophage vascular endothelial growth factor A production in an ARNT/HIF-dependent manner. *Infect Immun* 87:e00088-19. <https://doi.org/10.1128/IAI.00088-19>.
- Schwager S, Detmar M. 2019. Inflammation and lymphatic function. *Front Immunol* 10:308. <https://doi.org/10.3389/fimmu.2019.00308>.
- Mahnke A, Meier RJ, Schatz V, Hofmann J, Castiglione K, Schleicher U, Wolfbeis OS, Bogdan C, Jantsch J. 2014. Hypoxia in *Leishmania major* skin lesions impairs the NO-dependent leishmanicidal activity of macrophages. *J Invest Dermatol* 134:2339–2346. <https://doi.org/10.1038/jid.2014.121>.
- Colgan SP, Taylor CT. 2010. Hypoxia: an alarm signal during intestinal inflammation. *Nat Rev Gastroenterol Hepatol* 7:281–287. <https://doi.org/10.1038/nrgastro.2010.39>.
- Eltzschig HK, Carmeliet P. 2011. Hypoxia and inflammation. *N Engl J Med* 364:656–665. <https://doi.org/10.1056/NEJMra0910283>.
- Lin N, Simon MC. 2016. Hypoxia-inducible factors: key regulators of myeloid cells during inflammation. *J Clin Invest* 126:3661–3671. <https://doi.org/10.1172/JCI84426>.
- Fraga CA, Oliveira MV, Alves LR, Viana AG, Sousa AA, Carvalho SF, De Paula AM, Botelho AC, Guimaraes AL. 2012. Immunohistochemical profile of HIF-1alpha, VEGF-A, VEGFR2 and MMP9 proteins in tegumentary leishmaniasis. *An Bras Dermatol* 87:709–713. <https://doi.org/10.1590/s0365-05962012000500006>.
- Schatz V, Strussmann Y, Mahnke A, Schley G, Waldner M, Ritter U, Wild J, Willam C, Dehne N, Brune B, McNiff JM, Colegio OR, Bogdan C, Jantsch J. 2016. Myeloid cell-derived HIF-1alpha promotes control of *Leishmania major*. *J Immunol* 197:4034–4041. <https://doi.org/10.4049/jimmunol.1601080>.
- Araujo AP, Giorgio S. 2015. Immunohistochemical evidence of stress and inflammatory markers in mouse models of cutaneous leishmaniasis. *Arch Dermatol Res* 307:671–682. <https://doi.org/10.1007/s00403-015-1564-0>.
- Weinkopf T, Konrad C, Christian DA, Discher DE, Hunter CA, Scott P. 2016. *Leishmania major* infection-induced VEGF-A/VEGFR-2 signaling promotes lymphangiogenesis that controls disease. *J Immunol* 197:1823–1831. <https://doi.org/10.4049/jimmunol.1600717>.
- Carreau A, El Hafny-Rahbi B, Matejuk A, Grillon C, Kieda C. 2011. Why is the partial oxygen pressure of human tissues a crucial parameter? Small molecules and hypoxia. *J Cell Mol Med* 15:1239–1253. <https://doi.org/10.1111/j.1582-4934.2011.01258.x>.
- Lin N, Shay JES, Xie H, Lee DSM, Skuli N, Tang Q, Zhou Z, Azzam A, Meng H, Wang H, FitzGerald GA, Simon MC. 2018. Myeloid cell hypoxia-inducible

- factors promote resolution of inflammation in experimental colitis. *Front Immunol* 9:2565. <https://doi.org/10.3389/fimmu.2018.02565>.
24. McNamee EN, Korns Johnson D, Homann D, Clambey ET. 2013. Hypoxia and hypoxia-inducible factors as regulators of T cell development, differentiation, and function. *Immunol Res* 55:58–70. <https://doi.org/10.1007/s12026-012-8349-8>.
 25. Biddlestone J, Bandarra D, Rocha S. 2015. The role of hypoxia in inflammatory disease (review). *Int J Mol Med* 35:859–869. <https://doi.org/10.3892/ijmm.2015.2079>.
 26. Rao P, Suvas S. 2019. Development of inflammatory hypoxia and prevalence of glycolytic metabolism in progressing herpes stromal keratitis lesions. *J Immunol* 202:514–526. <https://doi.org/10.4049/jimmunol.1800422>.
 27. Via LE, Lin PL, Ray SM, Carrillo J, Allen SS, Eum SY, Taylor K, Klein E, Manjunatha U, Gonzales J, Lee EG, Park SK, Raleigh JA, Cho SN, McMurray DN, Flynn JL, Barry CE 3rd. 2008. Tuberculous granulomas are hypoxic in guinea pigs, rabbits, and nonhuman primates. *Infect Immun* 76:2333–2340. <https://doi.org/10.1128/IAI.01515-07>.
 28. Boutin AT, Weidemann A, Fu Z, Mesropian L, Gradin K, Jamora C, Wiesener M, Eckardt KU, Koch CJ, Ellies LG, Haddad G, Haase VH, Simon MC, Poellinger L, Powell FL, Johnson RS. 2008. Epidermal sensing of oxygen is essential for systemic hypoxic response. *Cell* 133:223–234. <https://doi.org/10.1016/j.cell.2008.02.038>.
 29. Evans SM, Schrlau AE, Chalian AA, Zhang P, Koch CJ. 2006. Oxygen levels in normal and previously irradiated human skin as assessed by EF5 binding. *J Invest Dermatol* 126:2596–2606. <https://doi.org/10.1038/sj.jid.5700451>.
 30. Jiang BH, Semenza GL, Bauer C, Marti HH. 1996. Hypoxia-inducible factor 1 levels vary exponentially over a physiologically relevant range of O₂ tension. *Am J Physiol* 271:C1172–C1180. <https://doi.org/10.1152/ajpcell.1996.271.4.C1172>.
 31. Kalgaard OM, Clausen OP, Mellbye OJ, Hovig T, Kvernebo K. 2011. Non-specific capillary proliferation and vasculopathy indicate skin hypoxia in erythromelalgia. *Arch Dermatol* 147:309–314. <https://doi.org/10.1001/archdermatol.2010.337>.
 32. Wong WJ, Richardson T, Seykora JT, Cotsarelis G, Simon MC. 2015. Hypoxia-inducible factors regulate filaggrin expression and epidermal barrier function. *J Invest Dermatol* 135:454–461. <https://doi.org/10.1038/jid.2014.283>.
 33. Ragnum HB, Vlatkovic L, Lie AK, Axcrone K, Julin CH, Frikstad KM, Hole KH, Seierstad T, Lyng H. 2015. The tumour hypoxia marker pimonidazole reflects a transcriptional programme associated with aggressive prostate cancer. *Br J Cancer* 112:382–390. <https://doi.org/10.1038/bjc.2014.604>.
 34. Zaidi M, Fu F, Cojocari D, McKee TD, Wouters BG. 2019. Quantitative visualization of hypoxia and proliferation gradients within histological tissue sections. *Front Bioeng Biotechnol* 7:397. <https://doi.org/10.3389/fbioe.2019.00397>.
 35. Viola A, Munari F, Sanchez-Rodriguez R, Scolaro T, Castegna A. 2019. The metabolic signature of macrophage responses. *Front Immunol* 10:1462. <https://doi.org/10.3389/fimmu.2019.01462>.
 36. Imtiyaz HZ, Simon MC. 2010. Hypoxia-inducible factors as essential regulators of inflammation. *Curr Top Microbiol Immunol* 345:105–120. https://doi.org/10.1007/82_2010_74.
 37. Hu CJ, Wang LY, Chodosh LA, Keith B, Simon MC. 2003. Differential roles of hypoxia-inducible factor 1alpha (HIF-1alpha) and HIF-2alpha in hypoxic gene regulation. *Mol Cell Biol* 23:9361–9374. <https://doi.org/10.1128/mcb.23.24.9361-9374.2003>.
 38. Lee KE, Simon MC. 2015. SnapShot: hypoxia-inducible factors. *Cell* 163:1288. <https://doi.org/10.1016/j.cell.2015.11.011>.
 39. Werth N, Beerlage C, Rosenberger C, Yazdi AS, Edelmann M, Amr A, Bernhardt W, von Eiff C, Becker K, Schafer A, Peschel A, Kempf VA. 2010. Activation of hypoxia inducible factor 1 is a general phenomenon in infections with human pathogens. *PLoS One* 5:e11576. <https://doi.org/10.1371/journal.pone.0011576>.
 40. Braverman J, Sogi KM, Benjamin D, Nomura DK, Stanley SA. 2016. HIF-1alpha is an essential mediator of IFN-gamma-dependent immunity to *Mycobacterium tuberculosis*. *J Immunol* 197:1287–1297. <https://doi.org/10.4049/jimmunol.1600266>.
 41. Doedens AL, Stockmann C, Rubinstein MP, Liao D, Zhang N, DeNardo DG, Coussens LM, Karin M, Goldrath AW, Johnson RS. 2010. Macrophage expression of hypoxia-inducible factor-1 alpha suppresses T-cell function and promotes tumor progression. *Cancer Res* 70:7465–7475. <https://doi.org/10.1158/0008-5472.CAN-10-1439>.
 42. Karaman S, Detmar M. 2014. Mechanisms of lymphatic metastasis. *J Clin Invest* 124:922–928. <https://doi.org/10.1172/JCI71606>.
 43. Phillips MB, Dina Zita M, Howells MA, Weinkopff T, Boehme KW. 2020. Lymphatic type 1 interferon responses are critical for control of systemic reovirus dissemination. *J Virol* 95:e02167–20. <https://doi.org/10.1128/JVI.02167-20>.
 44. Friedrich D, Zapf D, Lohse B, Fecher RA, Deepe GS, Jr, Rupp J. 2019. The HIF-1alpha/LC3-II axis impacts fungal immunity in human macrophages. *Infect Immun* 87:e00125-19. <https://doi.org/10.1128/IAI.00125-19>.
 45. Sulser P, Pickel C, Gunter J, Leissing TM, Crean D, Schofield CJ, Wenger RH, Scholz CC. 2020. HIF hydroxylase inhibitors decrease cellular oxygen consumption depending on their selectivity. *FASEB J* 34:2344–2358. <https://doi.org/10.1096/fj.201902240R>.
 46. Clausen BE, Burkhardt C, Reith W, Renkawitz R, Forster I. 1999. Conditional gene targeting in macrophages and granulocytes using LysMcre mice. *Transgenic Res* 8:265–277. <https://doi.org/10.1023/a:1008942828960>.
 47. Spath GF, Beverley SM. 2001. A lipophosphoglycan-independent method for isolation of infective *Leishmania* metacyclic promastigotes by density gradient centrifugation. *Exp Parasitol* 99:97–103. <https://doi.org/10.1006/expr.2001.4656>.
 48. Titus RG, Marchand M, Boon T, Louis JA. 1985. A limiting dilution assay for quantifying *Leishmania major* in tissues of infected mice. *Parasite Immunol* 7:545–555. <https://doi.org/10.1111/j.1365-3024.1985.tb00098.x>.